Check for updates

Original research article

Composites and Advanced Materials

Composites and Advanced Materials
Volume 35: 1–13
© The Author(s) 2026
Article reuse guidelines:
sagepub.com/journals-permissions
DOI: 10.1177/26349833261479739
journals.sagepub.com/home/acm
Sage

Radiation shielding performance and mechanical response of colemanite-modified cement-based composites

Hayrettin Eroğlu[1], Hasan Murat Çetin[2], and Felix N. Okonta[3]

Abstract

The need for non-toxic radiation-shielding composites has increased because conventional lead-based and heavyweight shielding solutions raise environmental, handling and structural-load concerns. This study aimed to evaluate whether thermally treated colemanite, a naturally occurring boron-rich mineral, can improve photon and neutron attenuation in a cement-based matrix while clarifying the associated mechanical penalty. Portland-cement composites containing 0, 1, 5 and 10 wt.% colemanite were prepared and tested for X-ray/gamma-ray mass attenuation, neutron attenuation, 7-day compressive strength, SEM morphology and XRD phase identification. Colemanite addition modified photon attenuation in an energy-dependent manner, with the strongest average low-energy improvement observed for the 5 wt.% mixture (+5.5% relative to the control). The effective linear neutron attenuation coefficient increased from 0.248 cm^{-1} for the control to 0.346 cm^{-1} for the 5 wt.% composite, whereas the highest density-normalized neutron attenuation value was obtained at 10 wt.% colemanite. This shielding benefit was accompanied by severe strength loss: 29.3%, 93.0% and 98.0% at 1, 5 and 10 wt.% colemanite, respectively. SEM and XRD findings indicate that colemanite was incorporated as a crystalline particulate phase, but heterogeneous dispersion and hydration interference governed the shielding-mechanical trade-off. The composites are therefore more suitable for non-load-bearing radiation-protective panels, partitions and surface layers than structural concrete applications.

Keywords

colemanite, cement-based composites, radiation shielding, neutron attenuation, gamma-ray attenuation, particulate mineral additive, SEM, XRD

Received: 15 June 2026; Revised: 7 July 2026; Accepted: 14 July 2026

1. Introduction

The rapid expansion of nuclear technologies in medical imaging, radiotherapy, industrial processing, radioactive-waste management and nuclear-service environments has increased the need for shielding materials that protect occupants and infrastructure from ionizing radiation.[1]

In such environments, shielding materials are no longer expected to perform only as passive radiation barriers. They must also be compatible with manufacturing, construction, durability, environmental and service requirements. This has shifted

[1]Department of Chemical Engineering, Faculty of Engineering and Architecture, Erzurum Technical University, Erzurum, Türkiye
[2]Department of Architecture, Building Information Division, Faculty of Architecture and Design, Atatürk University, Erzurum, Türkiye
[3]Department of Civil Engineering Science, University of Johannesburg, Johannesburg, South Africa

Corresponding author:
Hasan Murat Çetin, Department of Architecture, Building Information Division, Faculty of Architecture and Design, Atatürk University, Atatürk University Campus, Yakutiye, Erzurum 25240, Türkiye.
Email: hasanmurat.cetin@atauni.edu.tr

Creative Commons Non Commercial CC BY-NC: This article is distributed under the terms of the Creative Commons Attribution-NonCommercial 4.0 License (https://creativecommons.org/licenses/by-nc/4.0/) which permits non-commercial use, reproduction and distribution of the work without further permission provided the original work is attributed as specified on the SAGE and Open Access pages (https://us.sagepub.com/en-us/nam/open-access-at-sage).

research toward multifunctional composite systems in which radiation attenuation, matrix integrity and application-specific performance are considered together.[2,3]

Gamma and X-ray photons interact with matter mainly through the photoelectric effect, Compton scattering and pair production. The dominant interaction mechanism is controlled by photon energy, density, effective atomic number and elemental composition. Conventional shielding has therefore relied on lead, high-density alloys or heavyweight concrete. Lead is efficient but toxic and environmentally problematic, while heavyweight concrete can increase cost, component mass and construction constraints.[4–6]

Neutron shielding follows a different material logic. Fast neutrons are first moderated, commonly through scattering in hydrogen-bearing media, and then captured by nuclei with high neutron absorption cross sections. Boron-bearing materials are attractive because the ^{10}B isotope has a high thermal-neutron capture cross section and produces comparatively low-energy secondary radiation. Colemanite and related boron minerals have therefore been repeatedly considered as functional fillers for neutron-shielding materials.[7–10]

Recent studies on radiation-shielding concrete and advanced shielding composites show that attenuation performance cannot be interpreted only from chemical composition or density. Matrix type, filler dispersion, porosity, phase development, irradiation response and mechanical deterioration also govern the practical value of a shielding material. Cementitious and cement-bitumen composites containing waste glass, borate phases or other functional additives have been evaluated experimentally and through Monte Carlo-based approaches, demonstrating the importance of combining shielding measurements with mechanical and microstructural validation.[11–15]

The wider materials literature also shows that functional performance in modified composites is strongly affected by chemistry-microstructure-property coupling. Studies on molecular functional materials, nano-plastic-modified white cement pastes, asphalt binders modified with recycled rubber, cement-kiln-dust carbonation and CKD-based geopolymer production emphasize that additive-based material design must be assessed through integrated mechanical, microstructural and sustainability criteria rather than a single response variable.[16–20]

Cement-based composites provide a practical matrix platform because they are inexpensive, moldable and already used in building systems. However, conventional cementitious matrices have limited neutron attenuation and require modification by functional fillers or high-density phases. Boron-containing mineral additives are particularly relevant because they can contribute to neutron absorption while remaining natural, abundant and comparatively low-toxicity.[11,12,21,22]

Colemanite ($2CaO{\cdot}3B_2O_3{\cdot}5H_2O$) is a naturally occurring calcium borate mineral with a monoclinic crystal structure and a density of approximately 2.42 g/cm^3. Türkiye hosts major borate deposits, and colemanite has been examined in relation to boron-bearing construction, cement and shielding applications. Its boron-rich composition makes it relevant to neutron attenuation, while its particulate mineral form enables incorporation into cement-based composite matrices.[23–26]

Despite these advantages, an unresolved design problem remains: increasing boron-rich mineral content may improve neutron attenuation but may also retard cement hydration, disturb microstructural continuity and reduce early-age strength. This trade-off is critical for deciding whether colemanite-modified cement-based composites can be used as structural shielding concrete or should be restricted to non-load-bearing shielding components.[21,22,27–29]

Accordingly, the knowledge gap addressed in this study is the lack of an integrated evaluation of photon attenuation, neutron attenuation, microstructure and early-age mechanical response in colemanite-modified cement-based composites under the same experimental framework. The study is designed to clarify not only whether colemanite improves shielding, but also the mechanical and microstructural cost of that improvement.

1.1. Research objectives

The specific objectives of this study are: (i) to produce cement-based composite specimens incorporating 1, 5 and 10 wt.% thermally treated colemanite; (ii) to quantify their X-ray/gamma-ray mass attenuation coefficients and neutron attenuation coefficients; (iii) to evaluate the 7-day compressive-strength response and the strength loss associated with colemanite addition; (iv) to interpret the shielding-mechanical trade-off using SEM and XRD observations; and (v) to define realistic application windows for non-load-bearing radiation-protective composite components.

2. Materials and methods

2.1. Materials

Colemanite, a boron-rich mineral, was used as the functional particulate additive. Portland cement (CEM I 42.5 R), supplied by Aşkale Cement Factory, was used as the matrix binder. Colemanite was obtained from the Bigadiç district of Balıkesir,

Türkiye. Before incorporation into the cement matrix, the colemanite was ground, dried and sieved to obtain a particle-size distribution suitable for composite preparation.

Following grinding, the colemanite was thermally treated at 650 °C for 6 h in a muffle furnace to remove chemically bound water and improve dimensional and compositional stability during mixing. Mass measurements before and after treatment indicated that approximately 98% of the bound water was removed. Based on chemical analyses, the natural colemanite contained approximately 25.6% H_2O; after thermal treatment, the water content was reduced to approximately 1%.[26]

2.2. Preparation of cement-based composite specimens

Cement-based composite specimens were prepared in the Civil Engineering Laboratory at Erzurum Technical University. Four mixture groups were produced: one control mixture containing Portland cement and three colemanite-modified mixtures containing 1, 5 and 10 wt.% colemanite by binder weight.

The water-to-binder ratio was kept constant at 0.20 for all mixtures. The mixing water temperature was monitored with a digital thermometer and maintained between 25 and 30 °C. After mixing, the fresh pastes were cast into cubic molds with dimensions of 5 cm × 5 cm × 5 cm. The specimens were kept in the molds for 24 h, demolded and transferred to a controlled curing environment at 24 °C. Ambient temperature and relative humidity were monitored during curing.

2.3. X-ray and gamma-ray attenuation measurements

X-ray and gamma-ray attenuation measurements were conducted at the High Energy Spectroscopy Laboratory, Department of Atomic and Molecular Physics, Faculty of Science, Atatürk University. The measurement setup is schematically shown in Figure 1. A variable-energy VEX X-ray source and a Ba-133 radioisotope source were used as photon emitters. Photon intensity was measured before and after transmission through the cement-based composite specimens.

When a photon beam passes through an absorber of thickness t, the transmitted intensity decreases exponentially according to the Lambert-Beer law. The linear attenuation coefficient, μ, was calculated as:[4,27]

$$\mu = -(1/t)\ \ln(I/I_0) \tag{1}$$

where I is the transmitted photon intensity, I_0 is the incident photon intensity measured without the absorber, and t is the specimen thickness.

The mass attenuation coefficient, μ/ρ, was then obtained by normalizing the linear attenuation coefficient by the measured density, ρ:

$$\mu / \rho = -(1/\rho t)\ \ln(I/I_0) \tag{2}$$

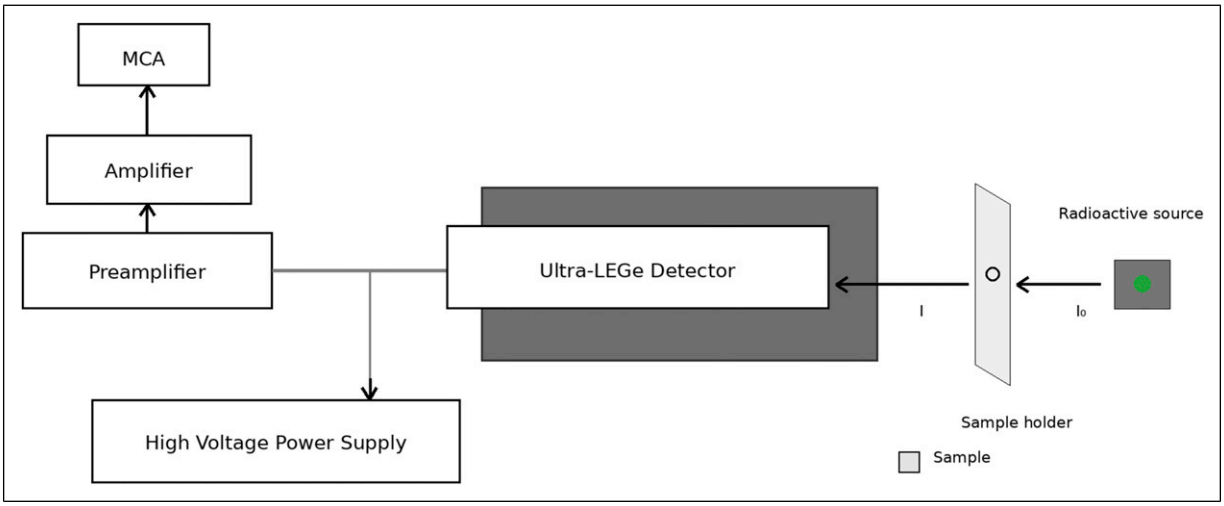


Figure 1. Schematic experimental setup for X-ray and gamma-ray attenuation measurements.

where ρt is the mass thickness of the absorber. The mass attenuation coefficient is expressed in cm^2/g and enables density-normalized comparison among the composite mixtures.[6,27]

2.4. Neutron attenuation measurements

Neutron attenuation measurements were carried out at the Prof. Dr. Gökhan Budak Neutron Measurement Laboratory, Department of Physics, Atatürk University. A ^{241}Am/Be source emitting fast neutrons in the energy range of approximately 2–11 MeV was used. Neutron detection was performed using a BF_3 gas-filled Canberra NP100B detector connected to Canberra ADM606 series digital counters. The experimental arrangement is schematically shown in Figure 2.[30,31]

The neutron attenuation behaviour was evaluated using an exponential attenuation relationship:

$$\Sigma = -(1/t)\ \ln(I/I_0) \tag{3}$$

where Σ is the effective linear neutron attenuation coefficient, I_0 is the incident neutron intensity, I is the transmitted neutron intensity and t is the specimen thickness. Because the ^{241}Am/Be source is polychromatic, the reported Σ should be interpreted as an effective, spectrum-averaged attenuation coefficient under the experimental geometry rather than a monoenergetic microscopic interaction parameter.[8,13,30–33]

The density-normalized neutron attenuation coefficient was calculated as:

$$\Sigma/\rho = -(1/\rho t)\ \ln(I/I_0) \tag{4}$$

where ρ is the measured density of the specimen. This parameter provides a density-normalized measure of neutron attenuation performance and is useful for comparing mixtures with different densities.[32,33]

2.5. X-ray diffraction analysis

X-ray diffraction (XRD) analysis was performed at the High Technology Application and Research Center (YUTAM), Erzurum Technical University, to identify crystalline phases and evaluate the incorporation of colemanite in the cementitious matrix.

2.6. Scanning electron microscopy analysis

Scanning electron microscopy (SEM) was conducted at YUTAM, Erzurum Technical University, to observe the microstructural morphology, particle distribution and pore characteristics of the control and colemanite-modified specimens.

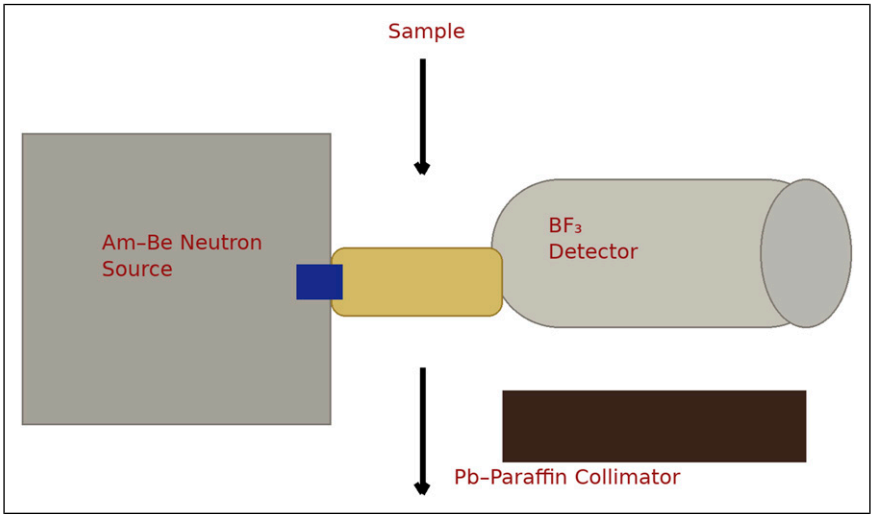


Figure 2. Schematic experimental setup for neutron attenuation measurements using a ^{241}Am/Be source and BF_3 detector.

2.7. Compressive strength test

The compressive strength of the cement-based specimens was determined at the Civil Engineering Laboratory of Erzurum Technical University according to TS EN 12390-3 (2019). Three specimens from each mixture were tested after 7 days of curing in saturated water conditions, and average compressive-strength values were reported.[34] The compressive-strength testing apparatus is shown in (Figure 3).

The compressive strength, σ, was calculated as:

$$\sigma = P / A \tag{5}$$

where P is the maximum load at failure and A is the loaded cross-sectional area.[35–37]

Because the available original test records contained only average compressive-strength values, inferential statistics such as standard deviation and analysis of variance could not be calculated without reconstructing unreported individual-specimen measurements. Accordingly, a descriptive effect-size analysis based on percentage changes relative to the control mixture is presented in the Results and Discussion section.

3. Results and discussion

3.1. X-ray and gamma-ray attenuation behaviour

Table 1 presents the X-ray and gamma-ray mass attenuation coefficients (μ/ρ, cm^2/g) of the control and colemanite-modified cement-based composites over the energy range of 13.375–385.851 keV. These values are reported as density-normalized photon attenuation coefficients, not as linear attenuation coefficients. The results show that colemanite addition modifies photon attenuation in an energy-dependent manner.

In the low-energy region of 13.375–24.942 keV, colemanite-modified specimens generally exhibited higher attenuation values than the control mixture. The average low-energy μ/ρ increased by 3.8% for 1 wt.% colemanite and by 5.5% for 5 wt.% colemanite relative to the control. The 10 wt.% mixture showed only a 0.3% average increase in this region, indicating that higher filler content did not produce a proportional photon-shielding gain.



Figure 3. Compressive strength testing apparatus used in the study.

Table 1. X-ray and gamma-ray mass attenuation coefficients, μ/ρ (cm^2/g), of colemanite-modified cement-based composites.

E (keV)	Control	Control + 1 wt.% colemanite	Control + 5 wt.% colemanite	Control + 10 wt.% colemanite
13.375	18.7	19.3	19.7	18.2
14.98	13.5	14	14.5	12.9
17.443	8.02	8.41	8.34	8.59
19.607	5.6	5.94	6.06	6.11
22.103	4.16	4.25	4.21	4.26
24.942	2.87	2.97	2.96	2.97
43.737	0.58	0.601	0.532	0.61
44.47	0.575	0.595	0.526	0.604
50.391	0.596	0.617	0.547	0.626
53.155	0.521	0.479	0.511	0.492
59.537	0.243	0.292	0.299	0.3
81	0.236	0.289	0.298	0.282
276.39	0.16	0.162	0.176	0.165
302.85	0.154	0.159	0.164	0.173
356.01	0.153	0.16	0.163	0.17
385.851	0.148	0.141	0.144	0.156

In the medium-energy region of 43.737–81 keV, the 1 wt.% and 10 wt.% mixtures showed average increases of 4.4% and 5.9%, respectively, whereas the 5 wt.% mixture showed a slight average decrease of 1.4%. This non-monotonic behaviour indicates that photon attenuation is governed not only by additive content but also by dispersion, density, pore structure and local matrix continuity.

At higher photon energies of 276.39–385.851 keV, the relative differences among mixtures became smaller in absolute terms, but the 5 wt.% and 10 wt.% mixtures still showed average increases of 5.2% and 8.0%, respectively. This is consistent with the expected shift in dominant photon interaction mechanisms from photoelectric absorption toward Compton scattering, where electron density and density-normalized composition become more influential than the presence of a single additive phase.[4–6,15,27]

The photon results therefore support a limited but measurable contribution of colemanite to X-ray/gamma attenuation. The effect is composition- and energy-dependent rather than linearly proportional to colemanite content. This finding is consistent with previous shielding studies showing that the radiation response of composites depends on filler chemistry, matrix density, phase distribution and measurement energy.[11,12,14,15]

3.2. Neutron attenuation behaviour

The neutron attenuation results are shown in Table 2. Colemanite incorporation reduced the transmitted neutron intensity and increased the attenuation coefficients. The relative beam intensity I/I_0 decreased from 0.875 for the control mixture to 0.852, 0.850 and 0.845 for the 1, 5 and 10 wt.% colemanite composites, respectively.

The effective linear neutron attenuation coefficient increased from 0.248 cm^{-1} for the control to 0.280 cm^{-1} for 1 wt.% colemanite and reached its maximum value of 0.346 cm^{-1} for the 5 wt.% colemanite composite. This corresponds to a 39.5%

Table 2. Neutron attenuation test values of colemanite-modified cement-based composites.

Sample	Transmitted intensity, I	Relative intensity, I/I_0	Thickness, t (cm)	Mass, M (g)	Density, ρ (g/cm^3)	Σ (cm^{-1})	Σ/ρ (cm^2/g)
Control	0.886	0.875	0.540	9.9676	1.8245	0.248	0.136
Control + 1 wt.% colemanite	0.863	0.852	0.570	9.9618	1.7274	0.280	0.162
Control + 5 wt.% colemanite	0.861	0.850	0.470	9.9564	2.0939	0.346	0.165
Control + 10 wt.% colemanite	0.856	0.845	0.550	9.9637	1.7906	0.306	0.171

increase relative to the control. The 10 wt.% mixture exhibited a lower effective linear coefficient of 0.306 cm^{-1}, but still remained 23.4% above the control value.

The density-normalized neutron attenuation coefficient (Σ/ρ) increased from 0.136 cm^2/g for the control to 0.162, 0.165 and 0.171 cm^2/g for the 1, 5 and 10 wt.% mixtures, respectively. Therefore, the 10 wt.% mixture provided the highest density-normalized neutron attenuation, while the 5 wt.% mixture provided the highest thickness-normalized attenuation. This distinction is important for design: a fixed-thickness barrier and a mass-constrained component may favour different mixture ratios (Table 2).

The improved neutron attenuation is attributed primarily to the boron content of colemanite, especially neutron capture by ^{10}B. The experimental trend is consistent with reports on colemanite, ulexite, tincal and borate-containing shielding systems evaluated using experiments and FLUKA or Monte Carlo simulations. However, direct numerical comparison must be made cautiously because neutron source spectrum, shielding thickness, detector response, matrix chemistry and density differ across studies.[8–10,13]

The present data do not constitute a new Monte Carlo simulation study. Instead, the comparison with the literature validates the physical direction of the response: boron-bearing phases improve neutron attenuation, but the magnitude of the measured coefficient is geometry- and matrix-specific. This limitation is explicitly acknowledged because the $^{241}Am/Be$ source provides a broad neutron spectrum rather than a monoenergetic beam.[13,30,32,33]

3.3. Early-age compressive strength and descriptive performance analysis

The 7-day compressive-strength results are summarized in Table 3 and plotted in Figure 4. The control specimen reached 30.32 MPa, whereas the incorporation of 1 wt.% colemanite reduced compressive strength to 21.43 MPa. This corresponds to a 29.3% reduction and indicates that even low colemanite addition can partially interfere with early-age cement hydration.

The strength reduction became severe at higher additive contents. The 5 wt.% colemanite composite reached only 2.11 MPa, corresponding to a 93.0% reduction relative to the control. The 10 wt.% mixture decreased further to 0.60 MPa, corresponding to a 98.0% strength loss and indicating near-complete loss of early-age load-bearing capacity.

This mechanical penalty is attributed mainly to the retarding effect of boron-containing compounds on cement hydration. Boron species can delay the hydration of C_3S and C_2S phases, limit C–S–H formation and weaken the cementitious matrix. Higher colemanite contents may also promote particle agglomeration, interfacial discontinuities and pore connectivity, thereby reducing load-transfer capacity.[21,28,29]

Table 4 summarizes the main descriptive changes relative to the control mixture. The data show that the largest increase in effective linear neutron attenuation (+39.5%) occurred at 5 wt.% colemanite, but this mixture also suffered a 93.0% compressive-strength loss. The 10 wt.% mixture offered the highest density-normalized neutron attenuation (+25.7%), but the strength loss increased to 98.0%. Therefore, the shielding improvement is not mechanically free; it is obtained by sacrificing the early-age integrity of the cementitious matrix.

From an application standpoint, these results rule out high-colemanite mixtures as structural concrete at early age. Their use is more defensible in non-load-bearing components, sacrificial shielding layers, internal radiation-protective partitions, surface-applied panels and prefabricated shielding units, where attenuation performance is prioritized and mechanical demand is limited or transferred to a separate structural frame.

3.4. SEM-based microstructural evaluation

SEM micrographs of the control and 5 wt.% colemanite specimens are shown in Figure 5. The control cement-based specimen exhibits a heterogeneous morphology with visible micro-pores and irregular particle distribution. Such features indicate local discontinuities in the matrix and limited interparticle packing.

Table 3. Seven-day compressive strength and relative strength loss of cement-based composite mixtures.

Colemanite content (wt.%)	Mixture	7-day compressive strength (MPa)	Strength loss relative to control (%)
0	Control	30.32	0.0
1	Control + 1 wt.% colemanite	21.43	29.3
5	Control + 5 wt.% colemanite	2.11	93.0
10	Control + 10 wt.% colemanite	0.60	98.0

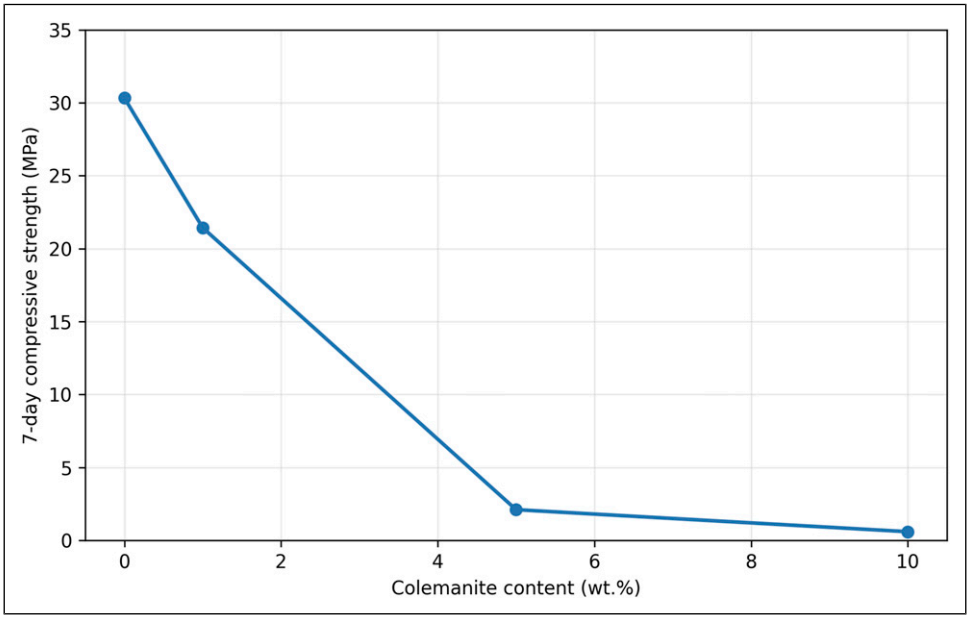


Figure 4. Seven-day compressive strength of colemanite-modified cement-based composites as a function of colemanite content.

The 5 wt.% colemanite-modified specimen displays a complex particulate microstructure. Colemanite particles appear embedded within the cementitious matrix and contribute to local filler effects. However, the micrographs also show heterogeneous particle distribution and localized agglomeration. These features support both sides of the observed performance trade-off: particulate incorporation contributes to radiation interaction pathways, whereas agglomeration and interfacial discontinuity reduce mechanical strength.

At higher magnifications, the microstructural contrast between the control and 5 wt.% colemanite specimen becomes more evident. The colemanite-added matrix contains particulate clusters and microstructural heterogeneities that can act as stress-concentration regions under compression. This observation is consistent with the significant decrease in compressive strength observed for the 5 wt.% formulation despite its superior neutron attenuation response.

The SEM evidence should be interpreted as morphological validation rather than a complete quantitative microstructural analysis. Additional image-based pore quantification, EDS mapping, mercury intrusion porosimetry or micro-CT would be required to quantify particle dispersion and pore connectivity in future work. Nevertheless, the SEM observations provide a physical explanation for why shielding enhancement and mechanical deterioration occur simultaneously.

3.5. XRD phase identification

The XRD pattern of the 5 wt.% colemanite-modified specimen is shown in Figure 6. The diffraction pattern confirms the presence of crystalline phases associated with the cementitious matrix and colemanite incorporation.

Table 4. Descriptive performance changes relative to the control mixture.

Mixture	Mean low-energy μ/ρ change (%)	Mean medium-energy μ/ρ change (%)	Mean high-energy μ/ρ change (%)	Σ change (%)	Σ/ρ change (%)	Strength loss (%)
Control	0.0	0.0	0.0	0.0	0.0	0.0
Control + 1 wt.% colemanite	+3.8	+4.4	+1.1	+12.9	+19.1	29.3
Control + 5 wt.% colemanite	+5.5	-1.4	+5.2	+39.5	+21.3	93.0
Control + 10 wt.% colemanite	+0.3	+5.9	+8.0	+23.4	+25.7	98.0

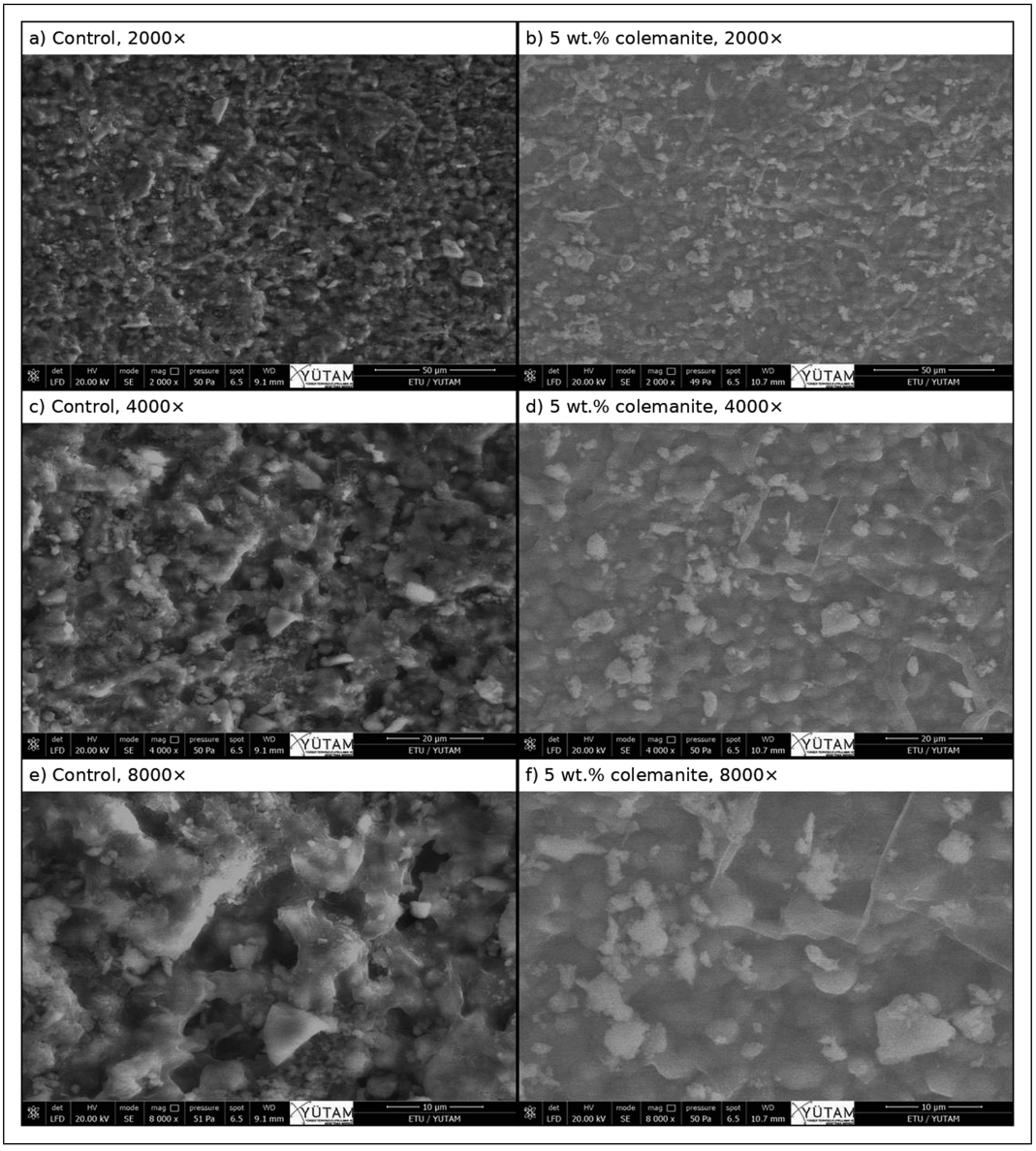


Figure 5. SEM micrographs of cement-based composites at different magnifications: (a), (c), (e) control specimen and (b), (d), (f) 5 wt.% colemanite-modified specimen at 2000x, 4000x and 8000x magnifications, respectively.

The intense peak around $2\theta \approx 29°$ is consistent with the characteristic crystalline response of colemanite, while additional peaks between approximately 35° and 50° are associated with typical hydrated Portland-cement phases, including portlandite and calcium-silicate-hydrate-related products. The coexistence of colemanite-related peaks and cement hydration phases supports successful incorporation of the mineral additive into the cement-based composite system.[23,24,28,29]

The XRD results complement the SEM findings by showing that colemanite remains as a crystalline, boron-rich particulate phase within the cementitious matrix. This phase can contribute to neutron attenuation, while the surrounding cementitious matrix provides shape stability and construction compatibility. At the same time, the XRD evidence does not contradict the observed strength loss, because the retention of crystalline colemanite can coincide with hydration retardation and heterogeneous microstructural development.

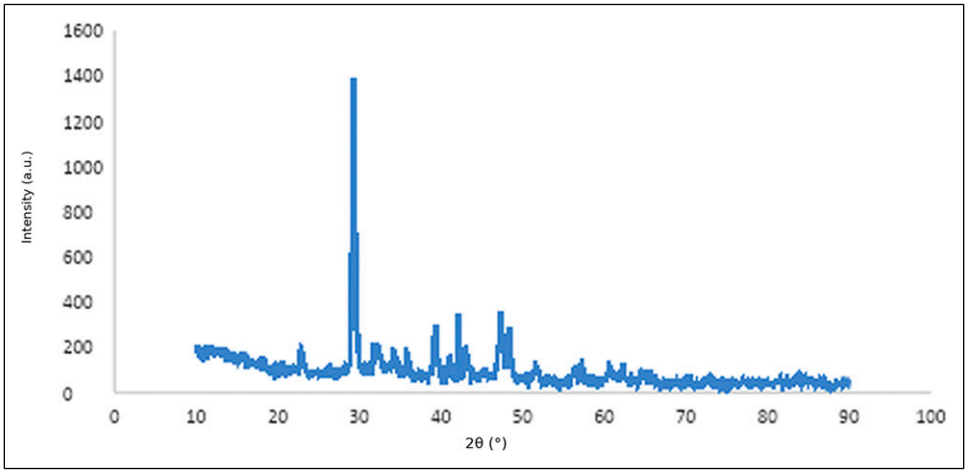


Figure 6. XRD pattern of the 5 wt.% colemanite-modified cement-based composite specimen.

3.6. Integrated mechanism, literature comparison and theoretical contribution

The theoretical contribution of this study is the explicit formulation of a shielding-mechanical trade-off for colemanite-modified cement-based composites. In this framework, colemanite acts as a boron-rich particulate functional filler that improves neutron attenuation primarily through boron-mediated capture processes and influences photon attenuation through composition-, density- and energy-dependent mechanisms. However, the same additive can retard cement hydration and disrupt microstructural continuity, which strongly reduces early-age strength at higher dosages.

This framework explains why a single optimum mixture cannot be defined without specifying the design objective. For a fixed-thickness neutron-shielding component, 5 wt.% colemanite is the most effective mixture in this study because it provides the highest effective linear neutron attenuation coefficient. For a mass-normalized neutron response, 10 wt.% colemanite is more efficient. For mechanical viability, 1 wt.% colemanite is safer but provides a smaller shielding gain. Therefore, mixture selection should be governed by the required balance among thickness, mass, attenuation and mechanical demand.

Compared with borate-containing barriers and cementitious shielding materials reported in the literature, the present results follow the expected direction: boron-rich phases improve neutron attenuation, while cementitious matrices can experience property deterioration when functional fillers interfere with hydration or microstructural continuity. Studies on borate waste isolation, waste-glass-modified cementitious matrices, cement-bitumen shielding composites and borosilicate shielding glass similarly demonstrate that radiation-shielding performance must be interpreted alongside mechanical and microstructural stability rather than as a standalone attenuation coefficient.[12–15]

The present work therefore contributes to composite-material design by identifying colemanite not as a universal structural enhancer, but as a function-specific particulate additive whose value depends on application constraints. This interpretation is more conservative than claiming structural radiation-shielding concrete, but it is more realistic for practical use in non-load-bearing shielding panels, protective partitions and surface layers integrated into radiation-sensitive buildings and facilities.

4. Conclusions

This study experimentally evaluated the radiation shielding performance and mechanical response of colemanite-modified cement-based composites. The findings show that colemanite can improve radiation attenuation, particularly neutron attenuation, but only at the cost of substantial early-age strength reduction at higher additive contents. The conclusions below are therefore framed in terms of theory, practice, lessons learnt and limitations rather than as a simple summary of results.

4.1. Implications to theory and practice

The results support the concept of colemanite as a boron-rich particulate functional filler in cement-based composites. The 5 wt.% mixture achieved the highest effective linear neutron attenuation coefficient (0.346 cm^{-1}), corresponding to a 39.5% increase relative to the control, while the 10 wt.% mixture achieved the highest density-normalized neutron attenuation

coefficient (0.171 cm^2/g). Photon attenuation was energy-dependent, with the strongest average low-energy improvement observed for the 5 wt.% mixture.

In practice, the composites should be considered primarily for non-load-bearing radiation-protective components rather than structural concrete. Relevant application routes include shielding panels, internal protective partitions, prefabricated radiation-protective units and surface layers for medical, laboratory and nuclear-service environments, where a separate structural system can carry load while the colemanite-modified composite contributes shielding functionality.

4.2. Key lessons learnt

The first key lesson is that higher colemanite content does not automatically produce a globally superior composite. The 5 wt.% mixture was best for effective linear neutron attenuation, but the 10 wt.% mixture was best for density-normalized neutron attenuation. The second lesson is that radiation performance must be read together with mechanical response: the 5 wt.% and 10 wt.% mixtures lost 93.0% and 98.0% of their 7-day compressive strength, respectively. The third lesson is that SEM and XRD evidence is essential for interpreting the mechanism, because particle incorporation, clustering and hydration-related heterogeneity explain why attenuation improvement and mechanical deterioration occurred together.

4.3. Limitations and future work

This study has several limitations. First, the compressive-strength analysis is based on available average values; individual specimen-level data were not available for statistical dispersion analysis. Second, the neutron attenuation coefficients are effective values measured under the present ^{241}Am/Be experimental geometry and should not be interpreted as mono-energetic nuclear constants. Third, the SEM and XRD results provide qualitative microstructural and phase validation, but not full quantitative phase, pore or particle-distribution analysis. Future studies should include longer curing ages, dispersion optimization, hybrid binder-filler systems, chemical admixture strategies to mitigate hydration retardation, quantitative SEM/EDS or micro-CT analysis and Monte Carlo modelling for geometry-independent comparison.

Within these limits, the study demonstrates that colemanite-modified cement-based composites are promising as sustainable, lead-free and non-load-bearing shielding materials, provided that their mechanical limitations are explicitly considered in design.

Acknowledgements

The authors acknowledge the laboratory infrastructure used for experimental measurements at Atatürk University and Erzurum Technical University.

ORCID iD

Hasan Murat Çetin https://orcid.org/0000-0001-8226-8243

Ethical considerations

This study did not involve human participants, human data, human tissue, animals, or clinical procedures. Ethics committee approval was therefore not required.

Author contributions

Conceptualization, H.E., H.M.Ç. and F.N.O.; methodology, H.E. and H.M.Ç.; validation, H.E., H.M.Ç. and F.N.O.; formal analysis, H.E. and H.M.Ç.; investigation, H.E.; resources, H.E.; data curation, H.E. and H.M.Ç.; writing - original draft, H.E.; writing - review & editing, H.E., H.M.Ç. and F.N.O.; visualization, H.E. and H.M.Ç.; supervision, H.E.; project administration, H.E. All authors reviewed and approved the final version of the manuscript.

Funding

The authors received no financial support for the research, authorship, and/or publication of this article.

Declaration of conflicting interests

The authors declared no potential conflicts of interest with respect to the research, authorship, and/or publication of this article.

Data Availability Statement

The source data supporting Tables 1–4 and Figure 4 are provided in the accompanying Microsoft Excel workbook, Supplementary Material 1. Additional data generated or analysed during the current study are available from the corresponding author upon reasonable request.

Supplemental material

Supplemental material for this article is available online.

References

1. International Atomic Energy Agency. *Radiation protection and safety of radiation sources: International basic safety standards*. Vienna: IAEA, 2014.
2. Akbulut S, Sehhatigdiri A, Eroğlu H, et al. A research on the radiation shielding effects of clay, silica fume and cement samples. *Radiat Phys Chem* 2015; 117: 88–92. https://doi.org/10.1016/j.radphyschem.2015.08.003
3. Eroğlu H, Yapıcı S and Varoğlu E. An investigation of the biosorption of radioactive gallium-67 in an aqueous solution using rose residue. *J Chem Eng Data* 2010; 55(8): 2848–2856. https://doi.org/10.1021/je901015a
4. Knoll GF. *Radiation detection and measurement*. 4th ed. John Wiley & Sons, 2010.
5. AbuAlRoos NJ, Baharul Amin NA and Zainon R. Conventional and new lead-free radiation shielding materials for radiation protection in nuclear medicine: A review. *Radiat Phys Chem* 2020; 165: 108439. https://doi.org/10.1016/j.radphyschem.2019.108439
6. Akkurt I, Akyıldırım H, Mavi B, et al. Gamma-ray shielding properties of concrete including barite at different energies. *Prog Nucl Energy* 2010; 52(7): 620–623. https://doi.org/10.1016/j.pnucene.2010.04.006
7. Lamarsh JR and Baratta AJ. *Introduction to nuclear engineering*. 3rd ed. Prentice Hall, 2001.
8. Korkut T, Karabulut A, Budak G, et al. Investigation of neutron shielding properties depending on number of boron atoms for colemanite, ulexite and tincal ores by experiments and FLUKA Monte Carlo simulations. *Appl Radiat Isot* 2012; 70(1): 341–345. https://doi.org/10.1016/j.apradiso.2011.09.006
9. Okuno K. Neutron shielding material based on colemanite. *Radiat Prot Dosimetry* 2005; 115: 258–261. https://doi.org/10.1093/rpd/nci154
10. Mesbahi A, Alizadeh G, Seyed-Oskoee G, et al. A new barite-colemanite concrete with lower neutron production in radiation therapy bunkers. *Ann Nucl Energy* 2013; 51: 107–111. https://doi.org/10.1016/j.anucene.2012.07.039
11. Onaizi AM, Amran M, Tang W, et al. Radiation-shielding concrete: A review of materials, performance, and the impact of radiation on concrete properties. *J Build Eng* 2024; 97: 110800. https://doi.org/10.1016/j.jobe.2024.110800
12. Maher A, Salama E, Mohamed RA, et al. Synergistic effects of lead borosilicate waste glass on the mechanical and radiation shielding properties of cement-bitumen composites. *Radiat Environ Biophys* 2025; 64: 505–517. https://doi.org/10.1007/s00411-025-01130-6
13. Bayoumi TA, Reda SM and Saleh HM. Assessment study for multi-barrier system used in radioactive borate waste isolation based on Monte Carlo simulations. *Appl Radiat Isot* 2012; 70(1): 99–102. https://doi.org/10.1016/j.apradiso.2011.09.016
14. Eid MS, Bondouk II, Saleh HM, et al. Investigating the effect of gamma and neutron irradiation on Portland cement provided with waste silicate glass. *Sustainability* 2023; 15(1): 763. https://doi.org/10.3390/su15010763
15. Ehab M, Salama E, Ashour A, et al. Optical properties and gamma radiation shielding capability of transparent barium borosilicate glass composite. *Sustainability* 2022; 14(20): 13298. https://doi.org/10.3390/su142013298
16. Banoon ZR, Al-Lami AKA, Abbas AM, et al. Asymmetrical liquid crystals synthesis for effective sensing: Fluorescence investigations. *Results Chem* 2023; 6: 101166. https://doi.org/10.1016/j.rechem.2023.101166
17. Abdelzaher MA, Farghali AA and Hamouda AS. Effective impact of nano-plastic-waste incorporated with nanotitina on the physical, mechanical and microstructural properties of white cement pastes composites for progressing towards sustainability. *Sci Rep* 2024; 14: 12581. https://doi.org/10.1038/s41598-024-62661-4
18. Owaid KA, Ghazal RY and Abdelzaher MA. Study of the effect of modification of asphalt on the rheological properties employing microwave radiation: An aging study. *Recycling* 2023; 8(5): 65. https://doi.org/10.3390/recycling8050065
19. Abdelzaher MA, Hamouda AS, Elkattan IM, et al. Laboratory study for accelerating the CKD mineral carbonation. *Egypt J Chem* 2022; 65(3): 491–499. https://doi.org/10.21608/ejchem.2021.93980.4425
20. Abbas R, Shehata N, Mohamed EA, et al. Environmental safe disposal of cement kiln dust for the production of geopolymers. *Egypt J Chem* 2021; 64(12): 7529–7537. https://doi.org/10.21608/ejchem.2021.89060.4276
21. Kula I, Olgun A, Erdoğan Y, et al. Effects of colemanite waste, coal bottom ash, and fly ash on the properties of cement. *Cem Concr Res* 2001; 31(3): 491–494. https://doi.org/10.1016/S0008-8846(00)00486-5
22. Sevim UK, Öztürk M, Bankir MB, et al. Utilization of colemanite waste in concrete design. *Int J Adv Eng Res Sci* 2017; 4(12): 172–175. https://doi.org/10.22161/ijaers.4.12.25

23. Anthony JW, Bideaux RA, Bladh KW, et al. *Handbook of mineralogy*. Mineralogical Society of America, 2003, vol 1.
24. Deer WA, Howie RA and Zussman J. *An introduction to the rock-forming minerals*. 3rd ed. Mineralogical Society, 2013.
25. Helvacı C. Geological features of Neogene basins hosting borate deposits: An overview of deposits and future forecast, Turkey. *Bull Miner Res Explor* 2015; 151: 169–215. https://doi.org/10.19111/Bmre.05207
26. Kocadağistan ME and Arslan H. Advantageous approach for boron ores used in cement production: Optimization of dehydration. *Challenge J Concr Res Lett* 2024; 15(1): 7–19. https://doi.org/10.20528/cjcrl.2024.01.002
27. Hubbell JH and Seltzer SM. *Tables of X-ray mass attenuation coefficients and mass energy-absorption coefficients 1 keV to 20 MeV for elements Z=1-92 and 48 additional substances of dosimetric interest*. National Institute of Standards and Technology, 2004. https://doi.org/10.18434/T4D01F
28. Taylor HFW. *Cement chemistry*. 2nd ed. Thomas Telford Publishing, 1997.
29. Scrivener KL, Juilland P and Monteiro PJM. Advances in understanding hydration of Portland cement. *Cem Concr Res* 2015; 78: 38–56. https://doi.org/10.1016/j.cemconres.2015.05.025
30. Krane KS. *Introductory nuclear physics*. John Wiley & Sons, 1988.
31. International Atomic Energy Agency. *Radiation, people and the environment*. Vienna: IAEA, 2004.
32. Wang P, Tang X, Chai H, et al. Design, fabrication, and properties of a continuous carbon-fiber reinforced Sm_2O_3/polyimide gamma ray/neutron shielding material. *Fusion Eng Des* 2015; 101: 218–225. https://doi.org/10.1016/j.fusengdes.2015.09.007
33. Singh VP and Badiger NM. Gamma ray and neutron shielding properties of some alloy materials. *Ann Nucl Energy* 2014; 64: 301–310. https://doi.org/10.1016/j.anucene.2013.10.003
34. Türk Standartları Enstitüsü. *Beton - Sertleşmiş beton deneyleri - Bölüm 3: Deney numunelerinde basınç dayanımının tayini (TS EN 12390-3)*. TSE, 2019.
35. Uzbaş B. *Çimento esaslı silis dumanlı uçucu küllü kompozitlerin SEM ve XRD destekli görsel analizlerinin yapay sinir ağları ile modellemesi*. PhD Thesis. Atatürk University, 2019.
36. Ustabaş İ. *Sülfat etkisine maruz mineral katkılı beton ve harçların performansının incelenmesi*. PhD Thesis. Karadeniz Technical University, 2008.
37. Sancak E. Borlu aktif belit çimentosu ile üretilen harçlarda kısa süreli donatı korozyonu davranışının araştırılması. *Sakarya Univ J Sci* 2015; 19(1): 89–98.